Observation of Fermi-edge excitons and exciton-phonon complexes in the optical response of heavily doped *n*-type wurtzite GaN

S. Shokhovets,[1,*] K. Köhler,[2] O. Ambacher,[2] and G. Gobsch[1]
[1]*Institute of Physics and Institute of Micro- and Nanotechnologies, Ilmenau University of Technology, PF 100565, 98684 Ilmenau, Germany*
[2]*Fraunhofer Institute for Applied Solid State Physics, Tullastr. 72, 79108 Freiburg, Germany*
(Received 22 August 2008; revised manuscript received 5 December 2008; published 6 January 2009)

We present the imaginary part of the dielectric function of *n*-type wurtzite GaN measured by spectroscopic ellipsometry in the spectral range of 3.2–4.5 eV at room temperature for electron concentrations from 1×10^{16} to 2.3×10^{19} cm^{-3}. The observed behavior is consistent with the Mott density of about 2×10^{18} cm^{-3}. The comprehensive line-shape analysis demonstrates the importance of excitonic effects over the whole doping range. For low electron concentrations, we observe contributions from discrete excitons, Coulomb enhanced band-to-band (BB) optical transitions, and transitions into exciton-phonon complexes (EPCs). For degenerate GaN, along with the BB transitions, we identify Fermi-edge excitons as well as a significant enhancement of the optical response due to EPCs. States with different numbers of phonons (from one to approximately ten) are active in such optical transitions in heavily doped GaN.

DOI: 10.1103/PhysRevB.79.045201 PACS number(s): 71.35.−y, 78.20.Ci, 78.20.Bh

I. INTRODUCTION

The concept of excitons plays an extremely important role in the understanding of the linear and nonlinear optical responses of semiconductors.[1] The linear response is described by the dielectric function (DF), $\varepsilon(E)=\varepsilon_1(E)+i\varepsilon_2(E)$, where E is the photon energy. In the present work we analyze the imaginary part of the DF of *n*-type wurtzite GaN close to the fundamental absorption edge. In this spectral range ε_1 is significantly larger than ε_2, and the $\varepsilon_2(E)$ spectrum bears great qualitative resemblance to the absorption spectrum. Throughout the whole paper the word(s) exciton (excitonic effects) will be used to point out the enhancement of the absorption rate of photons due to the Coulomb interaction between the photogenerated conduction-band electron (e) and valence-band hole (h) as compared with the independent-particle approximation, when the Coulomb e-h attraction and related effects are neglected. Of course, the usual meaning of the word exciton to denote a Coulomb-coupled e-h pair is also kept.

At low temperatures, the excitonic effects in samples of high crystal quality and low free-carrier concentration can be well described in the framework of Elliott's model.[2] As the temperature is increased, the discrete exciton lines become broadened and, in general, the excitonic contribution to the absorption decreases due to interactions between excitons and phonons. This lowering of the exciton oscillator strength was accounted for by a phenomenological factor f_x that depends on the ratio λ_p/a_x, where λ_p is the phonon mean-free path and a_x is the exciton Bohr radius.[3] For GaN, it was estimated that $f_x=0.97$ at room temperature, i.e., only a small decrease in the spectrally integrated excitonic absorption occurs in a temperature range of 0–300 K, though the broadening of optical transitions increases significantly.[3]

Much experimental and theoretical work was performed to understand free-carrier effects on the absorption edge of (i) optically excited semiconductors, (ii) quantum well structures, and (iii) bulk-doped semiconductors. Key aspects with relevance to the present paper are as follows:

(i) As the density of photoexcited carriers increases, the continuum edge moves downward on the energy scale (band-gap shrinkage), whereas the energy of the main excitonic peak remains almost unchanged until the bound exciton state merges with the continuum at a certain carrier density n_M which is called Mott density.[4–6] As revealed by extensive calculations,[7,8] the n_M value does not deviate very much from that calculated via

$$R_{SM}=0.84a_x. \tag{1}$$

Here, R_{SM} is the screening length corresponding to the insulator-metal (Mott) transition in an excitonic system, provided the effective e-h potential of $[-e^2/(4\pi\varepsilon_0\varepsilon_s r)\times\exp(-r/R_S)]$ (Yukawa potential) is assumed, where e is the elementary charge, ε_0 is the electric constant, ε_s is the static dielectric constant, and r is the e-h spacing. For this potential, the bound e-h states exist only if the screening length R_S is larger than R_{SM}.[9] It is essential that the oscillator strength of the bound exciton state is not much reduced until disappearing into the continuum.[7,10] Moreover, as revealed by experiments,[5,11] considerable enhancement of interband continuum transitions remains even at carrier concentrations well above the Mott density, though the sharp peak associated with excitons is no longer observed.

(ii) Realization of quantum well structures allowed for a comprehensive study of a dense two-dimensional electron gas, when the Fermi level is placed well above the conduction-band edge. Since the first experimental observation of the strong increase in photoluminescence intensity toward the electron Fermi energy for InGaAs-InP quantum wells by Skolnick *et al.*,[12] there have been numerous reports on the enhancement of optical transitions involving states near the Fermi level known as the Fermi-edge singularity (FES) or Mahan excitons (see, e.g., Refs. 13 and 14 for quantum wells based on III-V and II-VI semiconductors, respectively, and references therein). It was predicted by

Mahan[15] for metals that, due to the Coulomb interaction between the photogenerated electron and hole in the final state of the optical transition, the onset of the absorption spectrum should exhibit a power-law divergence. The underlying physics is that whenever the potential is switched on, the many-electron system responds by making a large number of elementary excitations with small excitation energies, which strongly affects the optical response. The role of temperature and finite lifetime of photogenerated *e-h* pairs is to broaden and suppress the edge anomaly.[16]

(iii) Experimental studies of the optical response of doped bulk semiconductors are in qualitative agreement with the results above. For example, according to Casey *et al.*,[17] the sharp excitonic peak which is observable in the absorption spectrum of high-purity GaAs disappears when an electron concentration of 5×10^{16} cm^{-3} is reached. At electron concentrations higher than $\sim6\times10^{17}$ cm^{-3}, the Burstein-Moss shift due to the filling of the conduction band (CB) by free electrons becomes the dominant effect. There are also several reports in which peculiar features in optical spectra of *n*-type-doped InAs bulk crystals,[18] as well as ZnO (Ref. 19) and InN (Ref. 20) epitaxial layers, were attributed to the FES.

A qualitative picture of excitonic effects as sketched above is more or less accepted at present.[1] However, many important details, for instance, the dynamics of screening,[6,21] exciton formation,[22] or conditions for the observation of FES,[13] are not completely clear and remain a subject of current research. No simple model for the absorption process exists.[23] Unlike high optical excitation when a nonequilibrium electron-hole plasma is formed or quantum wells where free carriers and dopants are usually spatially separated from each other, in a bulk-doped semiconductor free carriers and ionized impurities coexist in comparable amounts. This may affect, e.g., the screening of the Coulomb interaction between photogenerated electrons and holes because the free carriers are distributed inhomogeneously to provide the screening of ionized impurities.[24] A further aspect, which has been frequently ignored by calculations and interpretations of the optical response, is the enhancement due to optical transitions into exciton-phonon complexes (EPCs).[25] This mechanism is especially important for polar wide-band-gap semiconductors, such as GaN and ZnO, and is expected to be dependent on doping.

In this work we measured and analyzed the imaginary part of the DF of *n*-type wurtzite GaN up to an electron concentration of $n_e=2.3\times10^{19}$ cm^{-3}. The motivation for this analysis is to stress the importance of excitonic effects for the optical response of impure GaN, including heavy doping. The crucial point of our approach is the line-shape analysis allowing for the separation and quantifying of various contributions.

The paper is organized as follows. In Sec. II, GaN:Si samples and measurements of the DF by spectroscopic ellipsometry (SE) are described. Section III addresses first a qualitative consideration of the measured ε_2 spectra as a function of electron concentration. Then a model is introduced which allows an explicit analysis. Section IV describes details of band-to-band (BB) transitions for doped GaN at the specific carrier concentration of $n_e=3.7\times10^{18}$ cm^{-3}. It will be demonstrated that the nonparabolicity and nonsphericity of the valence band (VB) as well as the wave-vector-dependent probability of transitions into the CB are three important factors to determine the shape of the absorption edge due to BB transitions. Section V presents results of the line-shape analysis and their discussion. From the doping dependence of the measured ε_2 spectra, the Mott density of about 2×10^{18} cm^{-3} was derived. For degenerate GaN, in addition to the Coulomb-enhanced BB transitions, we identified Fermi-edge excitons and observed a significant enhancement of the optical response due to exciton-phonon complexes. Section VI gives a brief résumé of main results of this work. Throughout the paper we use parameters of wurtzite GaN summarized in Ref. 25. All calculations and discussions refer to the ordinary wave.

TABLE I. Characteristics of samples: the electron concentration, the Fermi energy counted from the conduction-band bottom, the expected broadening parameter due to fluctuation of the doping density, the width of the depletion layer, and the electric-field strength at the sample surface.

n_e (10^{18} cm^{-3})	ε_F (meV)	σ (meV)	w_0 (nm)	F_S (MV/cm)
0.01	−133.9	2.0	425	0.08
0.60	−27.1	11.1	52	0.59
1.1	−9.5	14.3	27	0.61
3.7	32.9	23.6	9.2	0.67
9.2	78.9	34.5	4.3	0.79
23	153.3	50.6	3.4	1.1

II. SAMPLES AND EXPERIMENTAL DETAILS

GaN:Si layers studied in this work are the same as in Ref. 26. For their growth, first a 25 nm GaN low-temperature nucleation layer followed by a 2 μm nominally undoped GaN buffer layer were deposited by low-pressure metal-organic vapor-phase epitaxy on *c*-plane sapphire substrates. The buffer layer was *n* type with a background electron concentration of about 1×10^{16} cm^{-3}. Then the GaN:Si layer was grown with five different Si doping concentrations N_{Si} ranging from 6.0×10^{17} to 2.3×10^{19} cm^{-3} (see Table I). Hall and secondary-ion mass spectrometry measurements showed that all Si atoms are on donor sites and are ionized at room temperature, i.e., $n_e=N_{\mathrm{Si}}$. In addition, it was observed[26] that the surface depletion region is formed, with the surface potential U_s and the width of the depletion layer w_0 depending on the Si concentration. In Table I, we show w_0 values determined in Ref. 26, as well as the electric-field strength at the sample surface F_s. The latter is estimated by $F_s=2U_s/w_0$ using the Schottky model according to which the electric-field strength decreases linearly within the depletion region.

The doping with Si should change the spectrum of BB transitions due to the band-gap narrowing (a redshift), the Burstein-Moss shift of the absorption edge (a blueshift), and the broadening of optical transitions. There are many reasons

TABLE II. Parameters of X-like and EPC-like bands determined from fits: magnitudes (A_X, A_{EPC}), energy positions (E_X, E_{EPC}), broadening parameters (σ_X, σ_{EPC}), as well as the average energy of phonons (ΔE_0) which are active in optical transitions into exciton-phonon complexes. For the meaning of quantities f_0, b, and N_m, please see the text.

n_e (10^{18} cm^{-3})	A_X	E_X (eV)	σ_X (meV)	σ_{EPC} (meV)	f_0	b	ΔE_0 (meV)	E_{EPC} (eV)	A_{EPC}	N_m
0.01	1	3.441	7.0	20	0.13	0.29	87	3.534	0.18	3.8
0.60	0.72	3.426	9.0	12	0.24	0.32	52	3.480	0.35	4.1
1.1	0.63	3.426	9.3	18	0.34	0.36	62	3.493	0.53	4.4
3.7	0.59	3.439	14	22	0.47	0.59	48	3.503	1.14	7.6
9.2	0.53	3.456	18	25	0.50	0.77	37	3.525	2.16	14.4
23	0.54	3.484	23	35	0.77	0.71	47	3.567	2.69	11.4

for the reduction in the band gap (see, e.g., Ref. 24). The most important phenomena which influence the renormalized band gap at high-enough densities of doping donors are the following: the exchange energy of electrons due to their fermionic nature, the attractive interaction between free electrons and charged donors, the exchange energy for holes, the repulsive interaction between holes and charged donors, the correlation energy of a hole due to rearrangement of electron density in its vicinity, and the band tailing caused by fluctuation of the doping density. To approximate the redshift with doping, in this work we use a simple empirical relation where the reduction in the band gap is assumed to be proportional to $n_e^{1/3}$ (see Sec. V). The Burstein-Moss shift of the absorption edge is observed when the Fermi level moves from the band gap into the CB. This results in a widening of an optical band gap. The effect depends on the position of the Fermi level ε_F with respect to the CB edge. ε_F values for the studied samples were calculated, taking into account the nonparabolicity of the CB of wurtzite GaN,[25] and are given in Table I. Regarding the broadening, the root-mean-square (rms) impurity potential $\sigma_0=[(e^4N_tR_S)/(8\pi\varepsilon_0^2\varepsilon_s^2)]^{1/2}$ is of importance,[27–29] where N_t is the total concentration of ionized impurities and their random distribution in the crystal is assumed. To incorporate the broadening into calculated ε_2 spectra, we use the Gaussian line-shape function $F(E,E_0,\sigma)=(2\sqrt{\pi}\sigma)^{-1}\exp[-(E-E_0)^2/(2\sigma)^2]$, where E_0 is the central (resonance) energy and E is the energy of an absorbed photon. In these notations, the full width at half maximum (FWHM) is equal to $4\sqrt{\ln 2}\sigma$. The broadening parameter σ due to fluctuation in the density of charged impurities is related to the rms impurity potential σ_0 by $\sigma=\sigma_0/\sqrt{2}$. Provided $N_t=n_e$, σ values quoted in Table I are obtained. If a correlated spatial distribution of impurities did exist at the growth temperature and this was "frozen in" during the cooling of the sample, the broadening observed by optical experiments at room or lower temperatures can be significantly smaller.[28] At present it is unclear whether such correlations in impurity distribution may occur because the growth temperature is low compared with the melting point of GaN.[30]

The surface morphology and structural properties of the samples were studied by atomic force microscopy (AFM) and high-resolution x-ray diffraction (HRXRD). In a 50×50 μm^2 AFM scan the rms surface roughnesses were 2.4 nm for an undoped sample and 1.9 nm for a 9.2×10^{18} cm^{-3} Si-doped sample. Although these values are quite similar, the slightly reduced surface roughness may be attributed to a decrease in threading dislocations by the Si doping.[31] From the HRXRD the undoped sample shows twist and tilt of 1000 and 300 arc sec, respectively. Quite similar values are found for the doped sample which shows twist and tilt of 1250 and 500 arc sec, indicating a comparable good structural quality of the doped and undoped samples. Optical studies confirmed this also. For example, the FWHMs of the discrete exciton line at room temperature are 23 and 31 meV for $n_e=1\times10^{16}$ cm^{-3} and $n_e=1.1\times10^{18}$ cm^{-3} samples, respectively (see σ_X parameters in Table II). The high structural and optical quality of the samples studied has the deciding significance regarding the determination of reliable data for the DF.

The DF was measured at room temperature by SE in a range of 3.2–4.5 eV with spectral resolution of about 5 meV. First, the DF of nominally undoped GaN buffer layer material was determined. These data were then used without change as the DF of the buffer layer in analyzing SE spectra of Si-doped samples. For each electron concentration, three samples with different thicknesses of the GaN:Si layer ranging from 150 nm to 1.5 μm were measured. The DF was obtained by a multiple-sample fit. Surface nonidealities (roughness and possible contamination) were modeled using a 50%/50% air/GaN Bruggeman effective medium. Since the c axis is normal to the sample surface, the procedure used yields the so-called isotropic DF. However, at room temperature and in the spectral range considered in this work, the isotropic DF is very close to the ordinary DF, as revealed by simulations considering the band structure of wurtzite GaN and typical geometry of SE measurements.[25,32] Therefore, the measured DF will further be treated as the ordinary one. The effect of the surface depletion layer will be discussed in Sec. V.

III. ε_2 SPECTRA AND MODEL

Figure 1(a) shows the measured (circles) ε_2 spectrum of nominally undoped GaN with electron concentration $n_e=1\times10^{16}$ cm^{-3}. The spectrum is very similar to that reported earlier for epitaxial layers with low electron concentration.[32] Analysis in Ref. 25 has revealed three contributing mechanisms: discrete excitons (X), Coulomb-enhanced BB transitions, and EPCs. Their partial contributions are shown in Fig.

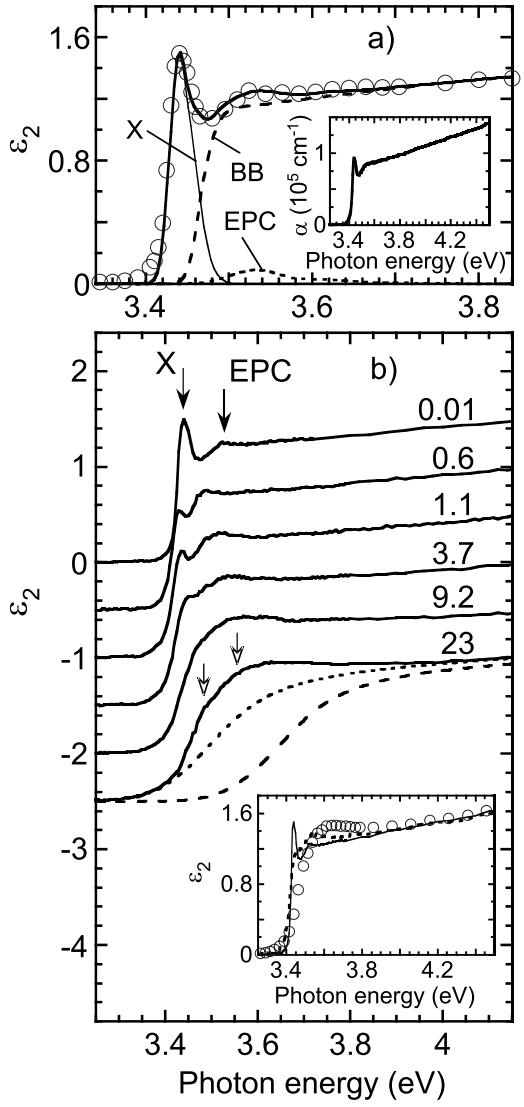

FIG. 1. (a) Measured (circles) imaginary part of the DF of undoped GaN and fit (thick solid line). Lines denoted by X, BB, and EPC show contributions of discrete excitons, band-to-band transitions, and transitions into exciton-phonon complexes, respectively. The inset presents the absorption coefficient determined from the measured DF. (b) Measured (solid lines) imaginary part of the DF for different electron concentrations. Curves are vertically displaced, for clarity. Numbers on the right indicate the electron concentration in units of 10^{18} cm^{-3}. The X and EPC bands of undoped GaN (solid arrows) are transformed into broader X-like and EPC-like bands for high electron concentrations (open arrows). For the meaning of dashed and dotted lines, see the text. In the inset, ε_2 spectra of 3.7×10^{18} (dotted) and 2.3×10^{19} cm^{-3} (circles) samples are compared to the spectrum of undoped GaN (thin solid line).

1(a) by the thin solid, dashed, and dotted lines, respectively, while the thick solid line represents the fit to the experimental data. The inset of Fig. 1(a) shows the absorption coefficient α determined from the measured DF. As mentioned in Sec. I, there is a qualitative resemblance between α and ε_2 spectra in a region close to the band gap. However, explicit quantitative details of the absorption spectrum depend also on the spectrum of the real part of the DF.

In Fig. 1(b) we reproduce the experimental ε_2 spectrum for nominally undoped material and show the results (solid lines) for five different electron concentrations. For clarity, curves for GaN:Si are vertically displaced downward with a step of 0.5. As seen, the effect of doping is to change the shape of the absorption edge, as well as to shift it slightly to the low-energy side and then to higher energies, when the electron concentration exceeds $\sim3\times10^{18}$ cm^{-3}.

Our quantitative analysis of this behavior is based on the experimental finding that the ε_2 curves for doped samples approach the $n_e=1\times10^{16}$ cm^{-3} curve at photon energies above 4 eV, i.e., ε_2 values in this spectral range are independent of the electron concentration within an experimental error of $\pm3\%$. This important feature is illustrated in the inset of Fig. 1(b) by comparison of 3.7×10^{18} and 2.3×10^{19} cm^{-3} samples to undoped GaN. A similar observation was made for the absorption coefficient of doped GaAs in the above-band-gap spectral region.[17,33,34] This means that, despite large changes in the optical response immediately at the absorption edge, the Coulomb enhancement of BB transitions persists.

As mentioned previously it follows that the free-carrier screening of the Coulomb attraction between the photoexcited electron and hole in the final state of the optical BB transition is negligibly small even if the free-carrier concentration is in excess of the Mott density. The observation of no (or low) screening may be qualitatively explained as follows. In a doped n-type semiconductor, for each ionized donor there is exactly one electron in the CB (we assume no compensation). The electrons are distributed about the donors to provide a steady-state screening. If a new photoexcited e-h pair arises, a certain time is required for the electron-donor system to respond. When a photon of energy E is absorbed, the electron and hole are created with kinetic energy $E-E_g$, where E_g is the band-gap energy. If this kinetic energy is small, the particles move slowly and the electron-donor system reacts instantaneously to the electron-hole position, i.e., the e-h interaction will be screened. However, for fast particles there is insufficient time to screen their electric field and the Coulomb e-h attraction is not changed from its unscreened value. Hence, the Coulomb enhancement of optical transitions persists. Similar observations were also reported for highly (above the Mott density) photoexcited GaAs (Ref. 11) and Ge.[5]

Based on the persistence of the Coulomb enhancement, as discussed above, we calculate the contribution of BB transitions for doped GaN in the same manner as it was done for GaN with low electron concentration in Ref. 25. The only modification needed is to take into account the occupation of CB and VB states by introducing a factor $\{f[E_{v\sigma_v}(\mathbf{k})]-f[E_c(\mathbf{k})]\}$, where f is the Fermi-Dirac distribution function, $\mathbf{k}$ is the wave vector of the photogenerated electron and hole, $E_c(\mathbf{k})$ is the CB dispersion relation, and $E_{v\sigma_v}(\mathbf{k})$ is the dispersion relation for holes belonging to the valence subband v ($v=A$, B, or C) with the spin variable $\sigma_v=\pm$. As mentioned in Sec. II, the ordinary imaginary part of the DF is calculated and compared with experiment in this work. Then, according to Eq. (1) of Ref. 25, the contribution of BB transitions is expressed as follows:

$$\varepsilon_{2,\mathrm{BB}}^{\perp}(E) = \frac{A_0 m_0 E_P^{\perp}}{16\pi^2 E^2} \sum_{v,\sigma_v} \int_{\mathrm{BZ}} [1 + f_x(S_v - 1)]\{f[E_{v\sigma_v}(\mathbf{k})] - f[E_c(\mathbf{k})]\} F_{v\sigma_v}^{\perp}(\mathbf{k})\, \delta[E_c(\mathbf{k}) - E_{v\sigma_v}(\mathbf{k}) - E] d\mathbf{k}, \tag{2}$$

with

$$S_v = (2\pi/\sqrt{\varepsilon_v})/[1 - \exp(-2\pi/\sqrt{\varepsilon_v})], \tag{3}$$

where the superscript $\perp$ denotes quantities related to the ordinary wave, $A_0 = (\hbar^2 e^2)/(\varepsilon_0 m_0^2)$, $\hbar$ is the Planck constant, m_0 is the free-electron mass, $E_P^{\perp}$ is the interband momentum matrix element in energy units, S_v is the Sommerfeld factor, $F_{v\sigma_v}^{\perp}(\mathbf{k})$ is the relative transition probability,[25] $\varepsilon_v = (E - E_{gv})/E_{bv}$, E_{gv} is the energy gap between the CB and the VB v at $\mathbf{k}=0$, and E_{bv} is the exciton binding energy of the exciton series belonging to the VB v.

The dashed line in Fig. 1(b) shows the calculated contribution of BB transitions for the highest electron concentration studied, with the band-gap energy being taken to be the same as for undoped GaN. As seen, the calculated absorption edge is placed much higher than the measured one, indicating a considerable band-gap narrowing. Reducing the band gap by 0.15 eV results in the dotted curve. Comparison to the experimental ε_2 spectrum reveals that the shape of the absorption edge cannot be accounted for by the Coulomb-enhanced BB transitions alone. Additional contributions are evident, which are indicated by open arrows and will further be called X-like and EPC-like optical transitions.

Now we introduce the model for the line-shape analysis of ε_2 spectra of doped GaN. The contribution of BB transitions is calculated by Eqs. (2) and (3). We will assume that the energy spacings between the A, B, and C VBs as well as the dispersion relations in the CBs and the VBs are doping independent. Then, only the band-gap energy E_{gA} is an adjustable parameter to be derived by comparison with experiment. X-like and EPC-like transitions are modeled in terms of two line-shape functions which were used in Ref. 25 for GaN with low electron concentrations to describe discrete excitons and exciton-phonon complexes. The former line-shape function consists of contributions from ground and excited states of the A, B, and C excitons [see Eq. (2) of Ref. 25]. In undoped GaN with low electron concentration, the position of discrete exciton lines with respect to the band gap E_{gv} is specified by the exciton binding energy E_{bv}. It is easy to see in Fig. 1(b) that the X-like band does not follow the continuum edge as the electron concentration increases. Therefore, for the sake of describing X-like transitions, we reformulate Eq. (2) of Ref. 25 by introducing an additional parameter E_{Gv} that plays the role of an effective optical band gap to which the X-like band is coupled in doped GaN. It is assumed that the energy spacing between E_{Gv} values ($v=A$, B, or C) is identical to that for E_{gv} regardless of the electron concentration. Then, the contribution of X-like transitions is expressed as follows:

$$\varepsilon_{2,\mathrm{X}}^{\perp}(E) = A_{\mathrm{X}} f_x \frac{A_0 m_0 E_P^{\perp}}{2E^2} \left(\frac{8\pi\varepsilon_0\varepsilon_s}{e^2}\right)^3 \sum_v \sum_{n=1}^{\infty} F_{v\perp}^{\mathrm{DX}} \left(\frac{E_{bv}}{n}\right)^3 \times \delta\left(E - E_{Gv} + \frac{E_{bv}}{n^2}\right), \tag{4}$$

where A_{X} is the normalized magnitude of the X-like band (i.e., $A_{\mathrm{X}}=1$ by definition for undoped GaN), $F_{v\perp}^{\mathrm{DX}}$ is the relative oscillator strength of excitons belonging to the VB v for undoped GaN,[25] and n is the principal quantum number associated with a given excitonic transition. Note that, according to Eq. (4), the relative oscillator strength of A, B, and C excitons which form the X-like band is given by the product $A_{\mathrm{X}} F_{v\perp}^{\mathrm{DX}}$, with the dependence on doping being carried over the parameter A_{X} to be deduced from fits to experimental data (see Table II for the determined A_{X} values). For low electron concentrations, $E_{Gv}=E_{gv}$ is fulfilled, whereas $E_{Gv} > E_{gv}$ should be expected for doped GaN. In the latter case, E_{GA} and E_{gA} values are treated as independent adjustable parameters to be determined from comparison of calculated and measured ε_2 spectra. After having calculated the contribution of X-like transitions, the effect of EPC-like transitions is modeled as multiphonon ($N=1,2,3,\ldots$) replicas of the X-like contribution scaled by a factor $(f_0/A_{\mathrm{X}})b^{N-1}$ and shifted to higher energies by $N\Delta E_0$, where ΔE_0 corresponds to a phonon energy. Quantities f_0 and b are discussed in Sec. V and their values are provided in Table II.

The broadening is incorporated into calculated ε_2 spectra using the Gaussian line-shape function (see Sec. II). Fits to experimental data revealed that BB, X-like, and EPC-like transitions are described by different broadening parameters σ_{BB}, σ_{X}, and σ_{EPC}, respectively. As Fig. 1(a) shows, discrete states of individual excitons are not resolved at room temperature and a slightly asymmetrical band results for X-like transitions with the peak at some photon energy E_{X} between A and B excitons. The asymmetry is mainly caused by the reduced oscillator strength of B and C excitons compared to the A exciton. Note that for the extraordinary wave, the shape of an X-like band would be different. The contribution of EPC-like transitions is small for undoped GaN [see the dotted line in Fig. 1(a)]. However, it is strongly enhanced in degenerately doped GaN, with the EPC band becoming quite broad and strongly asymmetric [see ε_2 spectrum for $n_e = 2.3 \times 10^{19}$ cm^{-3} sample in Fig. 1(b)]. As Secs. IV and V will demonstrate, the procedure presented above provides an accurate description and quantifying of doping effects on the optical response in a uniform manner over the whole range of electron concentrations.

Finally we quote the fitting parameters. These are the band-gap energies E_{gA} and E_{GA}, the magnitude A_{X} of the X-like band, the quantities f_0, b, and ΔE_0 to describe the EPC-like band, as well as the broadening parameters σ_{X} and σ_{EPC} for X-like and EPC-like transitions, respectively. Note that E_{GA} is a formal parameter in our model, and only E_{X} values will be discussed below. The Fermi energy is taken from Table I. To achieve good fit to experimental data at photon energies above 4 eV, a slight adjustment of the momentum matrix element $E_P^{\perp}$ was needed for different samples. However, the $E_P^{\perp}$ variations are well within experi-

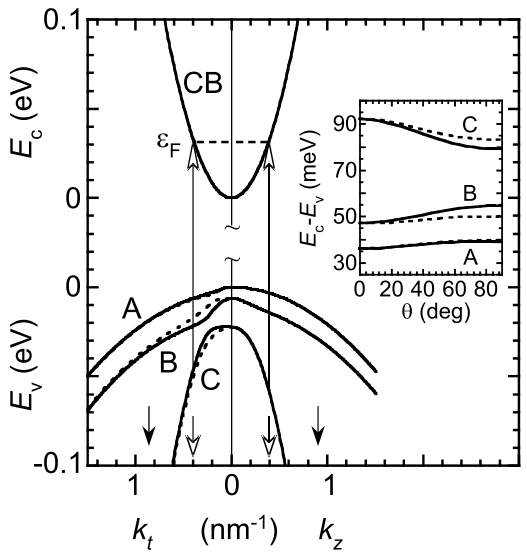

FIG. 2. Band structure of wurtzite GaN. The k_t (k_z) axis corresponds to wave vectors perpendicular (parallel) to the optic axis. Upper and lower valence subbands (Ref. 25) are shown by solid and dotted lines, respectively. Short open and filled arrows indicate wave vectors of free electrons at the Fermi level for electron concentrations of 3.7×10^{18} and 2.3×10^{19} cm^{-3}, respectively. Long open arrows denote direct optical transitions from the valence band into the conduction-band Fermi-level states for the electron concentration of 3.7×10^{18} cm^{-3}. The inset shows that, for each valence subband, the absorbed photon energy is a function of the angle between the wave vector and the optic axis.

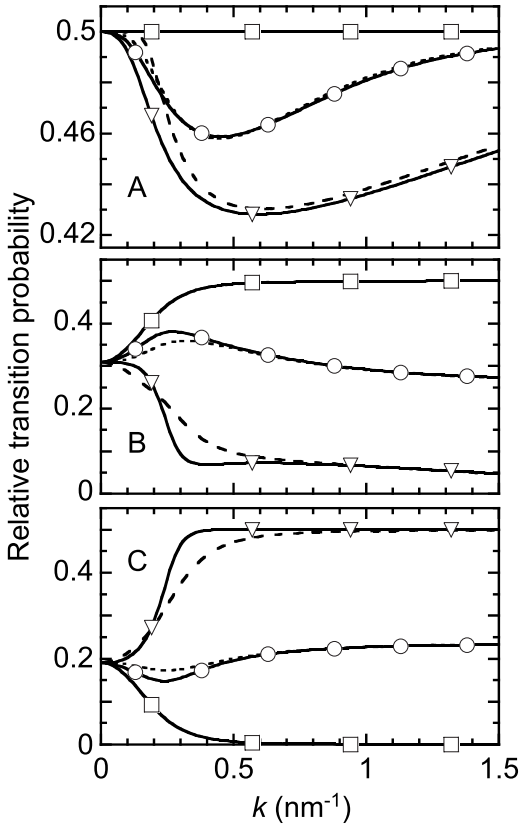

FIG. 3. Relative probability of direct optical transitions from *A* (top), *B* (middle), and *C* (bottom) valence bands into the conduction band for the ordinary wave as a function of the wave-vector length for three angles between the optic axis and the wave vector: squares for 0°, circles for 45°, and triangles for 90°. Solid lines superimposed on the symbols refer to upper valence subbands, while dotted and dashed lines stand for lower valence subbands (Ref. 25).

mental uncertainty of ε_2 values in this spectral range. As for the broadening of BB transitions for doped samples, fits allowing σ_{BB} to vary resulted in values close to σ in Table I. Therefore, $\sigma_{BB}=\sigma$ was taken for GaN:Si samples. Only for undoped GaN, the σ value is significantly smaller than the observed broadening, and σ_{BB} was set to be equal to σ_X (see Sec. V for more details).

IV. LINE-SHAPE ANALYSIS

Figure 2 shows the band structure of wurtzite GaN in the energy range responsible for the fundamental absorption edge. The lowest conduction band is doubly spin degenerate. Each of the three highest VBs (*A*, *B*, and *C*) is splitted into two subbands (except for the wave-vector direction parallel to the *c* axis). These subbands correspond to two possible values of the spin variable and are referred to as the upper valence subband and the lower valence subband (see Ref. 25 for more details). Owing to small values of the crystal-field and spin-orbit energies, all six valence subbands of wurtzite GaN are strongly nonparabolic and nonspheric near the zone center (see Fig. 2) and, in general, one might expect a nontrivial and concentration-dependent shape of the absorption edge due to direct BB transitions in doped crystals. In Fig. 2, short open and filled arrows indicate wave vectors of free electrons at the Fermi level for electron concentrations of 3.7×10^{18} and 2.3×10^{19} cm^{-3}. The long open arrows denote direct optical transitions from the VBs to the CB Fermi-level states for the former concentration. Note, for reference, that the $\varepsilon_F=0$ position of the Fermi level would correspond to $n_e=1.5\times10^{18}$ cm^{-3}. Below we address effects of different VBs on the shape of the absorption edge by an example of $n_e=3.7\times10^{18}$ cm^{-3}. The inset of Fig. 2 shows that the absorbed photon energy via transitions into the Fermi-level states of the CB is different for different valence subbands. Within each subband, there is a dependence on the angle θ between the wave vector and the optic (c) axis. This should result in smearing absorption edges belonging to different valence subbands. In addition, as Fig. 3 demonstrates, the transition probability depends very much on both the direction and the length of the wave vector, which is caused by a strong mixing of VB states at nonzero wave vectors. Thus, considering Figs. 2 and 3, one can conclude that, in general, contributions to the DF from different VBs and different **k** points of the Brillouin zone are very different. The essential point is, therefore, that the transition probability and the VB structure are to be treated together in order to calculate the actual shape of the absorption edge due to BB transitions.

In Fig. 4(a), contributions from *A*, *B*, and *C* VBs are shown by thin solid lines. Note that the Fermi surface is not sharply defined at room temperature. There are empty states even near the CB bottom. Applying the Coulomb enhancement results then in a steplike onset of the absorption at the

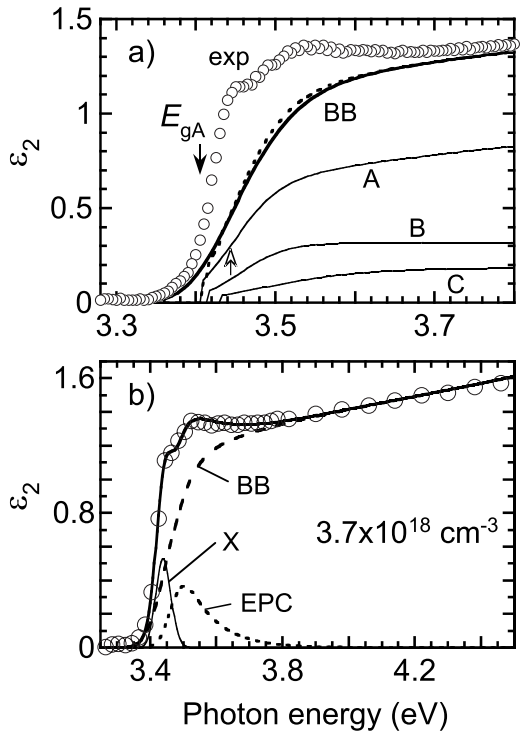

FIG. 4. (a) Contributions to the imaginary part of the DF due to band-to-band optical transitions from A, B, and C valence bands (thin solid lines), their sum without broadening (dotted line) and with incorporated broadening (thick solid line). The electron concentration is 3.7×10^{18} cm^{-3}. Filled and open arrows indicate the band-gap energy E_{gA} and an average photon energy for transitions from the VB A to the CB states at the Fermi level. For comparison, experimental data are shown by circles. (b) Fit (thick solid line) to the experimental data (circles). Three contributing mechanisms are caused by band-to-band (dashed line), X-like (thin solid line), and EPC-like (dotted line) optical transitions.

relevant band gaps. For clarity, filled and open arrows in Fig. 4(a) indicate the band-gap energy E_{gA} and an average photon energy for transitions from the VB A to the CB states at the Fermi level (see also Fig. 2). The dotted line in Fig. 4(a) denoted by BB is the sum of the A, B, and C contributions. Features due to the B and C VBs become hardly identifiable on this scale. Incorporating the broadening caused by fluctuations in distribution of impurities, which is quite large (see the σ parameter in Table I), results in the thick solid line which is practically structureless. Comparison to the experimental spectrum (circles) clearly demonstrates the existence of X-like and EPC-like transitions. The solid line in Fig. 4(b) is the fit to the experimental data using the model introduced in Sec. III. Contributions of partial mechanisms are also presented. Along with fitting parameters described in Sec. III, additionally the peak energy E_{EPC} of the EPC-like band, as well as the spectrally integrated strength of the X-like and EPC-like transitions were determined from this line-shape analysis. The spectrally integrated strength normalized to the spectrally integrated strength of discrete excitons for undoped GaN is given by A_{X} and $A_{\mathrm{EPC}}=f_0\Sigma_{N=1}^{\infty}b^{N-1}$ for X-like and EPC-like bands, respectively.

V. RESULTS AND DISCUSSION

Our main focus in this section is to discuss the electron-concentration dependence of the X-like and EPC-like bands and to explain their origin. First, however, remarks on the effect of the surface depletion layer on the measured DFs should be made. The magnitude of the absorption coefficient of GaN close to the absorption edge [see inset of Fig. 1(a)] implies that the penetration depth d_0 of light during SE experiments is slightly larger than 100 nm. This is considerably less than the width w_0 of the depletion region for nominally undoped GaN with $n_e=1\times10^{16}$ cm^{-3} (see Table I), which means that the electric-field strength does not change much within the penetration depth of light. Using F_S and w_0 values for this electron concentration from Table I as well as the d_0 value mentioned above, we see that the measured ε_2 spectrum corresponds to approximately 70 kV/cm which is below the ionization electric-field strength for excitons in GaN [~85 kV/cm (Refs. 35 and 36)]. Under such conditions, a slight shift to lower photon energies and field-induced broadening of discrete excitonic lines is expected as compared to the zero-field limit. Indeed, we observed for nominally undoped GaN that the broadening of X-like transitions σ_{X} significantly exceeds the expected broadening σ due to ionized impurities (compare Tables I and II). Note, however, that interactions with phonons are important at room temperature which can also be responsible for the observed σ_{X} value.

For $n_e\geq3.7\times10^{18}$ cm^{-3}, the inequality $d_0\gg w_0$ is fulfilled and the existence of a thin surface depletion layer may be ignored. Hence, the measured ε_2 spectra are characteristic of heavily doped GaN with nominal electron concentrations given in Table I.

With regard to $n_e=6\times10^{17}$ and 1.1×10^{18} cm^{-3} samples, the surface electric field is strong, while d_0 and w_0 are comparable, with d_0 being larger than w_0 (see Table I). As a result, high-, low-, and zero-field regions will contribute to the reflection and there are considerable spatial variations in the DF within the penetration depth of light. Generally speaking, a multilayer formalism[35] should be employed to extract the zero-field DF from the experimental SE data for these two electron concentrations. However, it would require a much more complicated analysis because electric-field effects on the DF of GaN can be treated only numerically.[36] In this work, we have not tried to take the presence of the depleted layer into a quantitative consideration.

Figure 5(a) presents the determined band-gap energy E_{gA} (squares) as well as peak positions E_{X} (triangles) and E_{EPC} (circles) of X-like and EPC-like bands as a function of electron concentration. The normalized spectrally integrated strength of X-like and EPC-like transitions is shown in Fig. 5(b). Other parameters determined from fits are given in Table II and in the inset of Fig. 5(b). The observed band-gap narrowing is described by $E_{gA}(n_e)=E_{gA}(0)-Kn_e^{1/3}$ with $E_{gA}(0)=3.478$ eV and $K=4.98\times10^{-8}$ eV cm [solid line in Fig. 5(a)]. K values from 1.3×10^{-8} to 5.7×10^{-8} eV cm have been reported from various experiments.[37–40] The discrepancy can be related to different experimental methods, crystal quality, and doping range studied. Peculiarities of Si incorporation and doping-dependent defect microstructure of samples also play a significant role.[39,41]

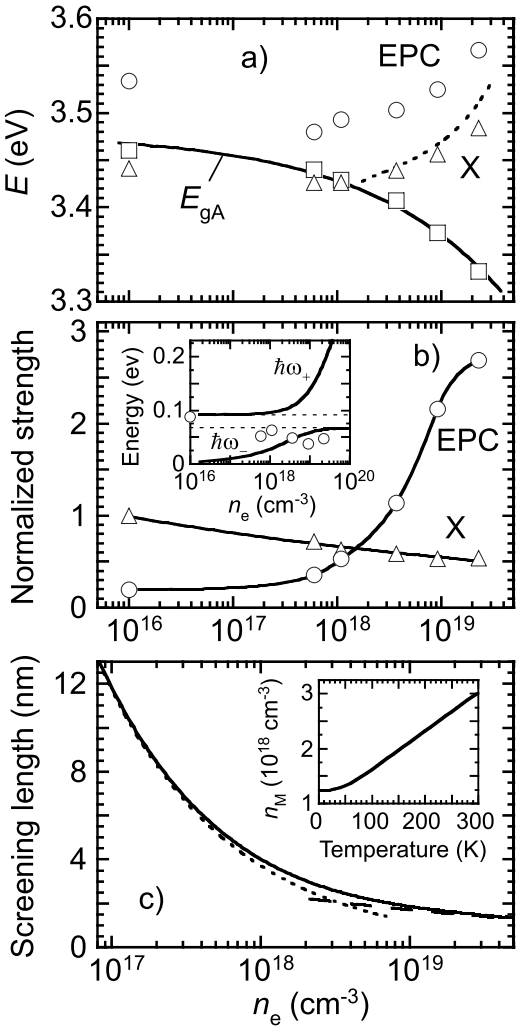

FIG. 5. (a) Band-gap energy (squares) and peak positions of X-like (triangles) and EPC-like (circles) bands as a function of electron concentration. The solid line is a fitting curve for the observed band-gap narrowing. The dotted line represents the expected doping-dependent one-particle absorption edge (see the text). (b) Electron-concentration dependence of the normalized spectrally integrated strength of X-like (triangles) and EPC-like (circles) bands. Solid lines are guide for the eyes. The inset shows two branches (solid lines) due to the plasmon-phonon coupling. Horizontal dotted lines indicate the energy of LO and TO phonons for undoped wurtzite GaN. Circles are the determined average energies of phonons that participate in optical transitions into exciton-phonon complexes. (c) Calculated screening length as a function of free-electron concentration for *n*-type wurtzite GaN at room temperature (solid line). Two commonly used approximations, Debye-Hückel and Thomas-Fermi screening lengths, are shown by dotted and dashed lines, respectively. The inset presents the temperature dependence of the Mott density calculated by applying criterion (1).

The X band for undoped GaN with $n_e=1\times10^{16}$ cm^{-3} lies 19 meV below the band gap (continuum edge) and, according to Ref. 25, is related to discrete excitons. The energy spacing between the X and EPC bands is close to the LO-phonon energy, and the EPC band is interpreted as optical transitions into exciton-phonon complexes. Parameters of the X and EPC bands for $n_e=1\times10^{16}$ cm^{-3} are given in Table II. They are in close agreement with those in Ref. 25. As the electron concentration is increased, there is initially a shift of the X-like band by 15 meV to the low-energy side for 6×10^{17} and 1.1×10^{18} cm^{-3} samples [see Fig. 5(a) and Table II]. As discussed in Sec. I, an approximately unchanged energy of excitonic resonance should be expected below the Mott density. We do not believe that the main reason for the observed decrease in peak energy of the X-like band is the presence of the depletion layer, although the Stokes shift of discrete exciton lines [which, however, does not exceed ~4 meV (Ref. 36)] and possible interference effects caused by electric-field inhomogeneities could affect peak positions and line shapes.[35] It is rather the effect of Si incorporation and related changes in the crystal microstructure (local strain, extended defects, etc.) that resulted in a noticeable redshift of the X-like band for 6×10^{17} and 1.1×10^{18} cm^{-3} samples with respect to undoped GaN. Note, however, that the energy gap between the X-like band and the continuum edge diminishes because the latter lowers more rapidly [see Fig. 5(a)]. When the electron concentration exceeds $\sim2\times10^{18}$ cm^{-3}, the X-like band moves into the continuum. The spectrally integrated strength of X-like transitions is the largest one for undoped GaN and gradually decreases as the doping density is increased [see Fig. 5(b) and Table II for the normalized strength which is equal to A_X, as discussed in Sec. IV]. In addition, the X-like optical transitions become progressively broader with increasing electron concentration (see σ_X parameters in Table II).

The observed behavior of the X-like band with increasing electron concentration agrees well with what should be expected for excitonic effects from studies of other semiconductors, as discussed in Sec. I. From this point of view, the free-electron concentration of $\sim2\times10^{18}$ cm^{-3} should be referred as the Mott density for wurtzite GaN at room temperature. Below we show that this value is close to the expected one from criterion (1). Assuming that the screening of the Coulomb attraction between photoexcited electrons and holes is caused by free electrons, the screening length is calculated by $R_S=[(e^2/\varepsilon_0\varepsilon_s)(dn_e/d\varepsilon_F)]^{-1/2}$, where ε_F is the Fermi energy (see, e.g., Ref. 42). The result for 300 K is presented in Fig. 5(c) by the solid line. For comparison, two commonly used approximations, known as the Debye-Hückel and Thomas-Fermi screening lengths, are shown by the dotted and dashed lines, respectively. As seen, both models underestimate the actual screening length in the intermediate range of electron concentrations and are only valid for low-density and high-density limits, respectively. With known screening length as a function of electron concentration, the Mott density n_M is derived by applying criterion (1). To calculate the temperature dependence of n_M shown in the inset of Fig. 5(c), the static dielectric constant, the exciton binding energy, and the exciton Bohr radius were linearly interpolated between their low-temperature ($\varepsilon_s=9.14$, $E_b=26.0$ meV, and $a_x=2.97$ nm) and room-temperature ($\varepsilon_s=9.60$, $E_b=23.6$ meV, and $a_x=3.12$ nm) values. The electron effective mass at the CB bottom ($m_{e0}=0.183m_0$) and coefficients of the CB nonparabolicity were assumed to be independent of temperature. More details about the parameters of wurtzite GaN can be found in Ref. 25. The calculation yields $n_M=3.0\times10^{18}$ cm^{-3} for 300 K which is in satis-

factory agreement with the experimental data of Fig. 5(a).

From high-excitation photoluminescence studies at low temperatures, Binet *et al.*[43] reported on significantly larger n_M values. Extrapolation of their data to room temperature would result in $n_M \sim 1\times10^{19}$ cm^{-3}. Note, however, that those data correspond to a threshold in the luminescence intensity on the high-energy side of the spectrum, and their physical meaning is different from that defined by criterion (1).

The dotted line in Fig. 5(a) is the expected one-particle absorption edge corresponding to direct optical transitions from the VB into the CB states at the Fermi level for $n_e > 1.5\times10^{18}$ cm^{-3}. As Fig. 4(a) shows, the contribution of the C VB to the DF is small compared to the A and B VBs. Therefore, considering a relatively small energy separation between the A and B VBs over the whole electron-concentration range studied (see Fig. 2) as well as smearing-out effects due to the VB nonsphericity, blurring of the Fermi surface at room temperature, and the broadening of optical transitions (see Sec. IV), we estimate the one-particle absorption edge by $E_{\mathrm{edge}}=E_c(\mathbf{k}_F)-[E_{A\sigma_v}(\mathbf{k}_F)+E_{B\sigma_v}(\mathbf{k}_F)]/2$, where $\mathbf{k}_F \| c$ was taken to calculate the dotted curve in Fig. 5(a). Note that valence A and B subbands are spin degenerate for this $\mathbf{k}$ direction and states with $\mathbf{k}$ directions near the optic axis dominate in optical transitions for the ordinary wave (see Fig. 3). The most striking feature of the X-like band is to follow the "classical" one-particle absorption edge for degenerate GaN. This is a strong argument for the interpretation of the observed enhancement of optical transitions (the X-like band) as Fermi-edge excitons, as first predicted by Mahan.[15] As seen in Fig. 5(b), the spectrally integrated strength of optical transitions due to Fermi-edge excitons shows only a weak doping dependence and amounts to approximately one-half of that for discrete excitons in undoped GaN.

In the following we address the EPC-like band which we account for by optical transitions into exciton-phonon complexes. This band is always well separated from and is considerably broader and asymmetrical than the X-like band [see Table II, as well as Figs. 1, 4, and 5(a)]. For example, the width of the high-energy side of the EPC band for $n_e=9.2\times10^{18}$ cm^{-3} is approximately twice the width of the low-energy side. In contrast to the X-like band, the spectrally integrated strength of the EPC-like band increases with increasing electron concentration [see Fig. 5(b)]. For degenerately doped GaN, the spectrally integrated contribution of EPC-like transitions even exceeds that of discrete excitons for undoped GaN. Below we interpret these features using the model described in Sec. IV. Within this model, the quantity ΔE_0 has a meaning of an average energy of phonons which participate in the coupling between the lattice and excitons. The quantity $f_0 b^{N-1}$ yields the normalized spectrally integrated strength of transitions via which a photon creates simultaneously exciton and N phonons, with f_0 being the normalized strength of the $N=1$ (one-phonon) transitions. The total normalized spectrally integrated strength of the EPC-like band is expressed as $A_{\mathrm{EPC}}=f_0\Sigma_{N=1}^{\infty} b^{N-1}$. These quantities can also be understood in terms of an exciton surrounded by a cloud of virtual phonons. In this case, the $(f_0/A_{\mathrm{EPC}})b^{N-1}$ value is interpreted as the partial contribution of a state with N phonons to a statistically averaged steady state of exciton-phonon complexes (see Ref. 25 for more details). For instance, Table II shows that, in contrast to undoped GaN, contributions of X-like transitions and EPC-like one-phonon transitions are comparable in degenerately doped GaN (compare A_{X} and f_0 values). The b parameter is a measure for the asymmetry of the EPC-like band, with a larger b resulting in a more asymmetrical band. The determined b value increases, while the ratio f_0/A_{EPC} decreases with increasing electron concentration, which clearly demonstrates an enhanced role of multiphonon states in the optical response of heavily doped GaN.

For a given electron concentration, the quantity b^{N-1} represents the relative contribution of a N-phonon replica with respect to that of the one-phonon replica. Since $b<1$ (see Table II), the contribution of multiphonon replicas decreases with increasing N. An estimation of the maximum number of phonons N_m to be effective in optical transitions into the EPCs can be obtained by setting $b^{N_m-1}=0.03$, i.e., the N_m-phonon replica is considered to make a 3% contribution. The latter is an experimental error in the determination of the DF (see Sec. III). All $N>N_m$ replicas are neglected. As seen in Table II, the determined N_m significantly increases with increasing electron concentration of up to $n_e=9.2\times10^{18}$ cm^{-3}. Afterward, there is an indication of a maximum (or saturation).

From polaron theory, where the interaction of electrons with lattice via LO phonons is assumed to be dominant, the average number of phonons in the cloud surrounding an electron is known to increase as the electron energy is increased.[44,45] Moreover,[46] a singularity (infinite average number of phonons in the polaron cloud) is expected when the kinetic energy of the electron approaches the LO-phonon energy [$\hbar\omega_{\mathrm{LO}}=91.5$ meV for wurtzite GaN (Ref. 25)]. If the electron kinetic energy exceeds $\hbar\omega_{\mathrm{LO}}$, the electron can emit a phonon, i.e., the interaction between the lattice and carriers changes drastically. Actually, the interaction of LO phonons with plasmons in a doped semiconductor leads to the split of the LO resonance into two branches $\hbar\omega_+$ and $\hbar\omega_-$ given by[47]

$$\omega_{\pm}^2=\frac{1}{2}(\omega_{\mathrm{LO}}^2+\omega_p^2)\pm\frac{1}{2}\sqrt{(\omega_{\mathrm{LO}}^2+\omega_p^2)^2-4\omega_p^2\omega_{\mathrm{TO}}^2}, \quad (5)$$

where $\hbar\omega_{\mathrm{TO}}$ is the TO-phonon energy, $\omega_p=[(n_e e^2)/\varepsilon_0\varepsilon_\infty m_e]^{1/2}$ is the plasmon frequency, ε_∞ is the high-frequency dielectric constant, and m_e is the electron effective mass. The result is shown in the inset of Fig. 5(b) by solid lines. (We used the momentum effective mass at the Fermi level as m_e for degenerate GaN.[25]) In consequence of the plasmon-phonon coupling, electric fields of LO phonons will be screened at large electron concentrations, and the phonon-like mode has a frequency ω_{TO}, not ω_{LO}. Then, having in mind the average number of phonons in the polaron cloud, the peculiar electron concentration is achieved if the Fermi energy is equal to $\hbar\omega_{\mathrm{TO}}$ [67.7 meV (Ref. 25)]. This would correspond to $n_e=7.6\times10^{18}$ cm^{-3}, which is somewhat lower than what the experiment yielded (see Table II). So far, however, we have not considered the second member of the photoexcited e-h pair—the photoexcited hole. On the one hand, the Fröhlich coupling constant of holes with the lattice in

GaN is larger than that of electrons.[25] As a result, a slow hole polaron has more phonons in its phonon cloud as compared to a slow electron polaron. On the other hand, owing to different effective masses, the kinetic energy of the hole belonging to an *e-h* pair created by a high-energy photon is significantly smaller than the kinetic energy of the electron. Then, considering an exciton-phonon complex as a sum of an electron polaron and a hole polaron, we expect that the peculiarity in the N_m dependence will be shifted to higher electron concentrations, in agreement with the experimental observation. This consideration indicates also that the rising role of exciton-phonon complexes in degenerate GaN is related to an enhanced coupling of a photoexcited *e-h* pair with the crystal lattice in the final stage of optical transition due to a high-energy photon. Owing to the increased kinetic energy of the photocreated electron and hole, states of the phonon cloud with different numbers of phonons (from 1 to $\sim N_m$) can be formed, which results in an increasing number of final states for the relevant optical transitions.

The above arguments account for the role of EPCs in the optical response of doped wurtzite GaN only in a qualitative manner. For example, it is unclear whether the phonon cloud of an exciton created by a high-energy photon may be treated as being made up of independent electron-polaron and hole-polaron clouds. In a rigorous presentation, all electrons and holes near the band edges should be replaced by polarons. Nonresonant and resonant polaron effects due to the interaction with optical phonons should be considered in a way similar to studies of GaAs and InP in an external magnetic field (see, e.g., Ref. 48 and references therein). Strong nonparabolicity and nonsphericity of the VB should also be of importance. A further complexity may arise from changes in the structure of the phonon cloud around the exciton as doping increases. To illustrate this, ΔE_0 values from Table II are shown in the inset of Fig. 5(b). For undoped GaN, ΔE_0 is close to the LO-phonon energy. At intermediate electron concentrations, ΔE_0 values may be explained as being due to the mixture of $\hbar\omega_+$ and $\hbar\omega_-$ modes. For degenerate samples, ΔE_0 is somewhat less than $\hbar\omega_{\mathrm{TO}}$. The latter can be attributed to a large average number of phonons in the phonon cloud around the exciton (see Table II). As a result, all long-wavelength optical phonons may be assumed to be involved in the coupling between the lattice and excitons. The effective average phonon energy will then be smaller as compared to the energy of screened LO phonons. A similar complicated structure of the phonon cloud around the exciton was also observed for ZnO.[25]

VI. SUMMARY

We measured the imaginary part of the DF of *n*-type wurtzite GaN with electron concentration from 1×10^{16} to 2.3×10^{19} cm^{-3} in the spectral range of 3.2–4.5 eV at room temperature. The comprehensive line-shape analysis showed that excitonic effects on the optical response are important in the whole doping range. For low electron concentrations, we observe contributions from discrete excitons, Coulomb enhanced BB optical transitions, and transitions into EPCs. In degenerate GaN, along with the Coulomb enhanced BB transitions, we identify Fermi-edge excitons and observe a significant enhancement of the optical response due to EPCs. The doping dependence of the measured ε_2 spectra indicates the Mott density of about 2×10^{18} cm^{-3}.

The Fermi-edge exciton band follows the classical one-particle absorption edge which would result from direct optical transitions from the valence band into the Fermi-level states of the conduction band. The broadening of the Fermi-edge exciton band increases with increasing free-electron concentration, while its spectrally integrated strength shows only a weak doping dependence and amounts to approximately one-half of the strength for discrete excitons in undoped GaN.

The EPC contribution is small at low electron concentrations. However, it is strongly enhanced for degenerately doped GaN. In addition, the EPC band becomes highly asymmetric. Our analysis of this behavior showed that states with different numbers of phonons (from one to approximately ten) are active in optical transitions into the EPCs in heavily doped GaN.

ACKNOWLEDGMENTS

We are indebted to the referee who focused our attention on the need for a more detailed consideration of the Mott density of wurtzite GaN. This work was supported by the Deutsche Forschungsgemeinschaft (Grants No. GO 586/6-1 and No. AM 105/5-1).

*Corresponding author; sviatoslav.shokhovets@tu-ilmenau.de

[1] C. Klingshirn, *Semiconductor Optics*, 2nd ed. (Springer, Berlin, 2005).
[2] R. J. Elliott, Phys. Rev. **108**, 1384 (1957).
[3] S. Shokhovets, G. Gobsch, and O. Ambacher, Phys. Rev. B **74**, 155209 (2006).
[4] G. W. Fehrenbach, W. Schäfer, J. Treusch, and R. G. Ulbrich, Phys. Rev. Lett. **49**, 1281 (1982).
[5] H. Schweizer, A. Forchel, A. Hangleiter, S. Schmitt-Rink, J. P. Löwenau, and H. Haug, Phys. Rev. Lett. **51**, 698 (1983).
[6] G. Manzke, Q. Y. Peng, K. Henneberger, U. Neukirch, K. Hauke, K. Wundke, J. Gutowski, and D. Hommel, Phys. Rev. Lett. **80**, 4943 (1998).
[7] R. Zimmermann, K. Kilimann, W. D. Kraeft, D. Kremp, and G. Röpke, Phys. Status Solidi B **90**, 175 (1978).
[8] H. Haug and S. Schmitt-Rink, Prog. Quantum Electron. **9**, 3 (1984).
[9] F. J. Rogers, H. C. Graboske, Jr., and D. J. Harwood, Phys. Rev. A **1**, 1577 (1970).
[10] J. G. Gay, Phys. Rev. B **4**, 2567 (1971).
[11] Jagdeep Shah, R. F. Leheny, and W. Wiegmann, Phys. Rev. B **16**, 1577 (1977).

[12] M. S. Skolnick, J. M. Rorison, K. J. Nash, D. J. Mowbray, P. R. Tapster, S. J. Bass, and A. D. Pitt, Phys. Rev. Lett. **58**, 2130 (1987).
[13] H. P. van der Meulen, I. Santa-Olalla, J. Rubio, J. M. Calleja, K. J. Friedland, R. Hey, and K. Ploog, Phys. Rev. B **60**, 4897 (1999); H. Kissel, U. Zeimer, A. Maassdorf, M. Weyers, R. Heitz, D. Bimburg, Y. I. Mazur, G. G. Tarasov, V. P. Kunets, U. Müller, Z. Y. Zhuchenko, and W. T. Masselink, *ibid.* **65**, 235320 (2002).
[14] D. Keller, D. R. Yakovlev, G. V. Astakhov, W. Ossau, S. A. Crooker, T. Slobodskyy, A. Waag, G. Schmidt, and L. W. Molenkamp, Phys. Rev. B **72**, 235306 (2005).
[15] G. D. Mahan, Phys. Rev. **153**, 882 (1967); **163**, 612 (1967).
[16] K. Ohtaka and Y. Tanabe, Rev. Mod. Phys. **62**, 929 (1990).
[17] H. C. Casey, Jr., D. D. Sell, and K. W. Wecht, J. Appl. Phys. **46**, 250 (1975).
[18] F. Fuchs, K. Kheng, P. Koidl, and K. Schwarz, Phys. Rev. B **48**, 7884 (1993).
[19] T. Makino, C. H. Chia, K. Tamura, Y. Segawa, M. Kawasaki, A. Ohtomo, and H. Koinuma, Phys. Rev. B **65**, 121201(R) (2002).
[20] M. Feneberg, J. Däubler, K. Thonke, R. Sauer, P. Schley, and R. Goldhahn, Phys. Rev. B **77**, 245207 (2008).
[21] Andrea Marini and Rodolfo Del Sole, Phys. Rev. Lett. **91**, 176402 (2003).
[22] W. Hoyer, M. Kira, and S. W. Koch, Phys. Rev. B **67**, 155113 (2003).
[23] G. Onida, L. Reining, and A. Rubio, Rev. Mod. Phys. **74**, 601 (2002).
[24] G. D. Mahan, J. Appl. Phys. **51**, 2634 (1980).
[25] S. Shokhovets, O. Ambacher, B. K. Meyer, and G. Gobsch, Phys. Rev. B **78**, 035207 (2008).
[26] K. Köhler, J. Wiegert, H. P. Menner, M. Maier, and L. Kirste, J. Appl. Phys. **103**, 023706 (2008).
[27] T. N. Morgan, Phys. Rev. **139**, A343 (1965).
[28] D. S. Domanevski and S. Shokhovets, Fiz. Tekh. Poluprovodn. (S.-Peterburg) **23**, 693 (1989) [Sov. Phys. Semicond. **23**, 434 (1989)].
[29] B. Arnaudov, T. Paskova, E. M. Goldys, S. Evtimova, and B. Monemar, Phys. Rev. B **64**, 045213 (2001).
[30] C. Kisielowski, in *Semiconductors and Semimetals*, edited by J. I. Pankove and T. D. Moustakas (Academic, San Diego, 1999) Vol. 57, p. 275.
[31] S. Ruvimov, Z. Liliental-Weber, T. Suski, J. W. Ager III, J. Washburn, J. Krueger, C. Kisielowski, E. R. Weber, H. Amano, and I. Akasaki, Appl. Phys. Lett. **69**, 990 (1996); Z. Benzarti, I. Halidou, O. Tottereau, T. Boufaden, and B. El Jani, Microelectron. J. **33**, 995 (2002).
[32] S. Shokhovets, G. Gobsch, and O. Ambacher, Appl. Phys. Lett. **86**, 161908 (2005).
[33] C. J. Hwang, J. Appl. Phys. **40**, 3731 (1969).
[34] G. B. Lush, M. R. Melloch, M. S. Lundstrom, H. F. MacMillan, and S. Asher, J. Appl. Phys. **74**, 4694 (1993).
[35] S. Shokhovets, D. Fuhrmann, R. Goldhahn, G. Gobsch, O. Ambacher, M. Hermann, U. Karrer, and M. Eickhoff, Appl. Phys. Lett. **82**, 1712 (2003); S. Shokhovets, D. Fuhrmann, R. Goldhahn, G. Gobsch, O. Ambacher, M. Hermann, and M. Eickhoff, Thin Solid Films **450**, 163 (2004).
[36] A. T. Winzer, G. Gobsch, R. Goldhahn, D. Fuhrmann, A. Hangleiter, A. Dadgar, and A. Krost, Phys. Rev. B **74**, 125207 (2006).
[37] In-Hwan Lee, J. J. Lee, P. Kung, F. J. Sanchez, and M. Razeghi, Appl. Phys. Lett. **74**, 102 (1999).
[38] M. Yoshikawa, M. Kunzer, J. Wagner, H. Obloh, P. Schlotter, R. Schmidt, N. Herres, and U. Kaufmann, J. Appl. Phys. **86**, 4400 (1999).
[39] Z. Chine, A. Rebey, H. Touati, E. Goovaerts, M. Queslati, B. El Jani, and S. Laugt, Phys. Status Solidi A **203**, 1954 (2006).
[40] H. P. D. Schenk, S. I. Borenstain, A. Berezin, A. Schön, E. Cheifetz, S. Khatsevich, and D. H. Rich, J. Appl. Phys. **103**, 103502 (2008).
[41] L. T. Romano, C. G. Van de Walle, J. W. Ager III, W. Götz, and R. S. Kern, J. Appl. Phys. **87**, 7745 (2000).
[42] P. Van Mieghem, G. Borghs, and R. Mertens, Phys. Rev. B **44**, 12822 (1991).
[43] F. Binet, J. Y. Duboz, J. Off, and F. Scholz, Phys. Rev. B **60**, 4715 (1999).
[44] T. D. Lee, F. E. Low, and D. Pines, Phys. Rev. **90**, 297 (1953).
[45] A. S. Mishchenko, N. V. Prokofev, A. Sakamoto, and B. V. Svistunov, Phys. Rev. B **62**, 6317 (2000).
[46] G. D. Mahan, *Many-Particle Physics* (Plenum, New York, 1993), p. 511.
[47] B. B. Varga, Phys. Rev. **137**, A1896 (1965); A. Mooradian and G. B. Wright, Phys. Rev. Lett. **16**, 999 (1966).
[48] P. Pfeffer and W. Zawadzki, Phys. Rev. B **53**, 12813 (1996).